GRB 011121: A Collimated Outflow into Wind-blown Surroundings

Greiner, J.; Klose, S.; Salvato, M.; Zeh, A.; Schwartz, R.; Hartmann, D.H.; Masetti, N.; Stecklum, B.; Lamer, G.; Lodieu, N.; Scholtz, R.D.; Sterken, C.; Gorosabel, J.; Burud, I.; Rhoads, J.E.; Mitrofanov, I.; Litvak, M.; Sanin, A.; Grinkov, V.; Andersen, M.I.; Cerón, J.M.; Castro-Tirado, A.J.; Fruchter, A.; Fynbo, J.U.; Hjorth, J.; Kaper, L.; Kouveliotou, C.; Palazzi, E.; Pian, E.; Rol, E.; Tanvir, N.R.; Vreeswijk, P.M.; Wijers, R.A.M.J.; van den Heuvel, E.P.J.

Published in:
Astrophysical Journal

DOI:
10.1086/379606

The Astrophysical Journal, 599:1223–1237, 2003 December 20

GRB 011121: A COLLIMATED OUTFLOW INTO WIND-BLOWN SURROUNDINGS[1]

J. Greiner,[2,3] S. Klose,[4] M. Salvato,[2,3] A. Zeh,[4] R. Schwarz,[2,5] D. H. Hartmann,[6] N. Masetti,[7] B. Stecklum,[4] G. Lamer,[2] N. Lodieu,[2] R. D. Scholz,[2] C. Sterken,[8] J. Gorosabel,[9,10] I. Burud,[10] J. Rhoads,[10] I. Mitrofanov,[11] M. Litvak,[11] A. Sanin,[11] V. Grinkov,[11] M. I. Andersen,[2] J. M. Castro Cerón,[12] A. J. Castro-Tirado,[9,13] A. Fruchter,[10] J. U. Fynbo,[14] J. Hjorth,[15] L. Kaper,[16] C. Kouveliotou,[17] E. Palazzi,[7] E. Pian,[18] E. Rol,[16] N. R. Tanvir,[19] P. M. Vreeswijk,[20] R. A. M. J. Wijers,[16] and E. van den Heuvel[16]

Received 2003 May 28; accepted 2003 September 2

ABSTRACT

We report optical and near-infrared follow-up observations of GRB 011121 collected predominantly at ESO telescopes in Chile. We discover a break in the afterglow light curve after 1.3 days, which implies an initial jet opening angle of about 9°. The jet origin of this break is supported by the fact that the spectral energy distribution is achromatic during the first 4 days. During later phases, GRB 011121 shows significant excess emission above the flux predicted by a power law, which we interpret as additional light from an underlying supernova. In particular, the spectral energy distribution of the optical transient approximately 2 weeks after the burst is clearly not of power-law type but can be presented by a blackbody with a temperature of ~6000 K. The deduced parameters for the decay slope and the spectral index favor a wind scenario, i.e., an outflow into a circumburst environment shaped by the stellar wind of a massive gamma-ray burst (GRB) progenitor. Because of its low redshift of $z = 0.36$, GRB 011121 has been the best example for the GRB-supernova connection until GRB 030329 and provides compelling evidence for a circumburster wind region expected to exist if the progenitor was a massive star.

Subject headings: gamma rays: bursts — supernovae: general — techniques: photometric

On-line material: color figures

1. INTRODUCTION

In the presently favored scenario for classical gamma-ray bursts (GRBs), occurring at cosmological distances (measured redshift range so far $0.36 < z < 4.5$; van Paradijs et al. 1997; Andersen et al. 2000), the explosion of a very massive star leads to a fireball and a short, beamed flash of gamma rays (Woosley 1993; Fryer, Woosley, & Hartmann 1999; Mészáros 2002), resulting in three physically distinct observational phenomena, namely, the GRB itself, a long-lasting afterglow, and the classical supernova (SN) light. Whereas the afterglow emission is probably fed by the kinetic energy of the collimated, relativistic outflow, the SN light is caused by the decay of radioactive nuclei created and released during the stellar explosion. The maximum of the SN light is expected at ~10–20$(1 + z)$ days after the explosion, although at present it is not clear whether or not the GRB and the SN explosion are delayed (Vietri & Stella 1998). One of the basic consequences of this hypernova scenario is that it predicts (and links) the occurrence of a GRB with a jet, the unavoidable strong wind from the massive progenitor star, and the SN light (Heger et al. 2003).

Earlier evidence on the GRB-SN connection was initially based on the coincidence of GRB 980425 and SN 1998bw (Galama et al. 1998), and subsequently some SN light contribution was found in the late-time light curves of GRB 980326 (Castro-Tirado & Gorosabel 1999; Bloom et al. 1999), GRB 970228 (Galama et al. 2000), and GRB 970508 (Sokolov 2002), as well as possibly GRB 980703 (Holland et al. 2001), GRB 990712 (Björnsson et al. 2001), GRB 991208 (Castro-Tirado et al. 2001), and GRB 000911 (Lazzati et al. 2001).

[1] Based on observations collected at the European Southern Observatory, La Silla and Paranal, Chile (ESO Programme 165.H-0464).
[2] Astrophysikalisches Institut, D-14482 Potsdam, Germany.
[3] Max-Planck-Institut für extraterrestrische Physik, Giessenbachstrasse Postfach 1603, D-85741 Garching, Germany.
[4] Thüringer Landessternwarte Tautenburg, Karl-Schwarzschild-Observatorium, Sternwarte 5, D-07778 Tautenburg, Germany.
[5] Universitäts-Sternwarte Göttingen, Geismarlandstrasse 11, D-37083 Göttingen, Germany.
[6] Department of Physics and Astronomy, Clemson University, 118 Kinard Laboratory, Clemson, SC 29634.
[7] Istituto di Astrofisica Spaziale e Fisica Cosmica, CNR, Sez. di Bologna, Via Gobetti 101, I-40129 Bologna, Italy.
[8] Vrije Universiteit Brussel, Astrofysisch Institute, Pleinlaan 2, B-1050 Brussels, Belgium.
[9] Instituto de Astrofísica de Andalucía (IAA-CSIC), Apartado Correos 3004, E-18080 Granada, Spain.
[10] Space Telescope Science Institute, 3700 San Martin Drive, Baltimore, MD 21218.
[11] Space Research Institute, Russian Academy of Sciences, Profsoyusnaya 84/32, 117810 Moscow, Russia.
[12] Real Instituto y Observatorio de la Armada, Sección de Astronomía, 11.110 San Fernando-Naval (Cádiz), Spain.
[13] Laboratorio de Astrofísica Espacial y Física Fundamental, Madrid, Spain.
[14] Institute of Physics and Astronomy, University of Aarhus, Ny Munkegade, DK-8000 Aarhus C, Denmark.
[15] Astronomical Observatory, Copenhagen University, Juliane Maries Vej 30, DK-2100 Copenhagen, Denmark.
[16] Universiteit van Amsterdam, Kruislaan 403, NL-1098 SJ Amsterdam, Netherlands.
[17] National Space Science and Technology Center, SD-50, 320 Sparkman Drive, Huntsville, AL 35805.
[18] Istituto Nazionale di Astrofisica, Osservatorio Astronomico di Trieste, Via Tiepolo 11, 34131 Trieste, Italy.
[19] Department of Physical Sciences, University of Hertfordshire, College Lane, Hatfield Herts AL10 9AB, UK.
[20] European Southern Observatory, Alonso de Cordova 3107, Vitacura, Casilla 19001, Santiago 19, Chile.

Observations of massive stars in our Galaxy have shown that they lose matter via strong stellar winds in the LBV and in the Wolf-Rayet evolutionary phase. GRB progenitors are expected to be very massive stars and perhaps physically related to Type Ib/c SNe (Heger et al. 2003). The progenitors of these stars should develop fast winds at the end of their lives and thus wind features are expected to be seen in afterglow light curves. The evolution of classical SN remnants into wind-blown bubbles has been a target of detailed investigations for years (e.g., Benetti et al. 1999; Landecker et al. 1999). What has been missing in GRB research until GRB 030329 (Hjorth et al. 2003), however, was a strong observational link between an underlying SN component in an afterglow light curve and evidence for a fireball expanding into a stellar wind profile. Significant work in this direction has been done over the past years by many groups from the theoretical, as well as observational, side (e.g., Mészáros, Rees, & Wijers 1998; Chevalier & Li 2000), and GRBs with wind-profile interactions have been identified in some cases, including GRB 980425/SN 1998bw (Chevalier & Li 2000). However, if one excludes GRB 980425 from this list, prior to GRB 011121 the observational database was rather poor. GRB 011121 changed this observational situation, although in a less spectacular way than GRB 030329. Not only was the distance of the burster relatively small, but also the light curve steepened 1 day after the burst so that a bright SN component became visible.

GRB 011121 was detected by the GRBM/WFC on board *BeppoSAX* on 2001 November 21, 18:47:21 UT and localized to initially 5′ (Piro 2001a). Subsequent analysis refined this position to 2′ accuracy (Piro 2001b), and the triangulation of the GRB arrival times as measured by *Ulysses*, *BeppoSAX* (Hurley et al. 2001), and the High Energy Neutron Detector (HEND; Hurley et al. 2002) further refined the coordinates. A follow-up X-ray observation with the *BeppoSAX* narrow-field instruments revealed a fading X-ray afterglow (Piro et al. 2001).

Follow-up optical/near-infrared (NIR) observations of GRB 011121 were quickly started by several groups, leading to independent discoveries of the afterglow (e.g., Wyrzykowski, Stanek, & Garnavich 2001; Greiner et al. 2001). Further observations revealed a rather small distance, $z \approx 0.36$ (Infante et al. 2001), and excess emission above the early power-law decay (Garnavich et al. 2001). The interpretation of this excess light as a possible SN bump attracted much attention and resulted in the so far best sampling of GRB afterglow emission at late times.

Here we report the results of observations obtained by the GRACE[21] (GRB Afterglow Collaboration at ESO) consortium.

2. OBSERVATIONS

2.1. *X-Rays/Gamma Rays*

The light curves of GRB 011121 measured with the two detectors of HEND are shown in Figure 1. Integrated into the Third Interplanetary Network, the *Mars Odyssey* satellite has two instruments with GRB detection capabilities: the Gamma-Ray Spectrometer and HEND. HEND combines four detectors to measure the spectra of neutrons and gamma rays (I. Mitrofanov et al. 2003, in preparation). In particular, the inner/outer CsI scintillators can measure gamma-ray photons in the 30–1000 keV range, at commandable integration times, and in case of a GRB trigger (or solar flare), time histories at 1.0/0.25 s resolution are recorded.

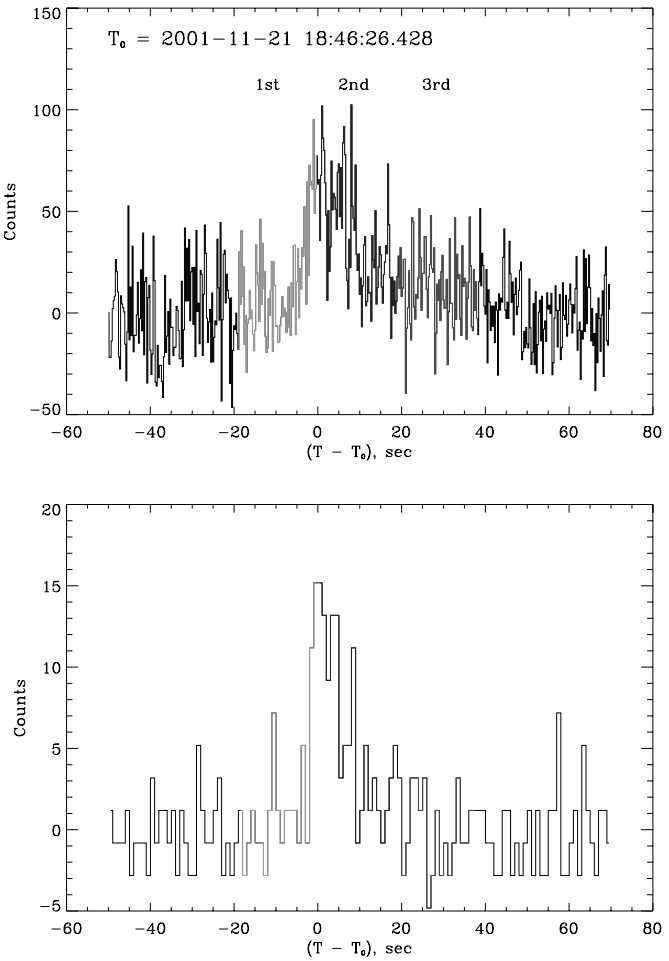

FIG. 1.—Light curve of GRB 011121 as recorded by HEND on *Mars Odyssey* in the outer scintillator at greater than 30 keV with 0.25 s time resolution (*top*) and in the inner scintillator at greater than 60 keV with 1 s time resolution (*bottom*). The time axis zero point (UT) is indicated at the top. The three colors represent the three successive time segments used for the spectral fitting (see Fig. 2). [*See the electronic edition of the Journal for a color version of this figure*.]

Figure 1 shows that the gamma-ray emission is characterized by a main peak with ~10 s duration, followed by a ~20 s tail. Thus, GRB 011121 clearly belongs to the long-duration subclass of GRBs.

According to the HEND energy spectra (Fig. 2), there is no obvious spectral evolution along the light curve of GRB 011121. All three 20 s segments of the time profile have spectra with the same power-law slope with a photon index of -2.35 ± 0.25 (after backward folding of the model with the instrument response). There is no evidence in the HEND data that the early afterglow emission started already at the time of the last segment of the burst.

Based on the power-law spectral slope of 2.35, the fluence is $(2 \pm 0.4) \times 10^{-5}$ ergs cm^{-2} in the 250–700 keV range. This corresponds to an (isotropic) energy release of $E = 2.7 \times 10^{52}$ ergs at the given redshift (luminosity distance of 2.07

[21] See http://zon.wins.uva.nl/~grb/grace.

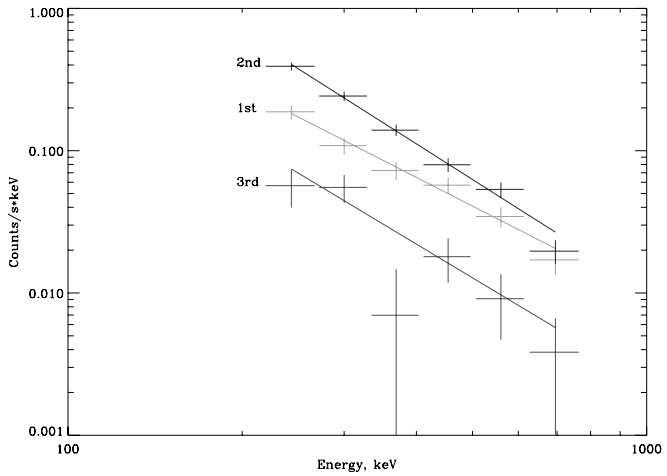

FIG. 2.—Energy spectra of GRB 011121 above 200 keV, as recorded by HEND on *Mars Odyssey* in the outer scintillator for three successive time segments, shown as green, blue, and red in the light curve (see Fig. 1). [*See the electronic edition of the Journal for a color version of this figure.*]

Gpc) and the cosmological parameters $\Omega_\Lambda = 0.7$, $\Omega_M = 0.3$, and $H_0 = 65\ \mathrm{km\ s^{-1}\ Mpc^{-1}}$.

2.2. *Optical and NIR Imaging*

About 9 hr after the GRB, K_s- and R-band images were obtained at La Silla (ESO) with SOFI (equipped with a 1024×1024 HAWAII array with 18.5 μm pixels and a plate scale of $0\farcs29$ pixel^{-1}) at the 3.58 m New Technology Telescope (NTT) and with EFOSC2 (equipped with a 2048×2048 thinned Loral/Lesser CCD with 15 μm pixels and a plate scale of $0\farcs157$ pixel^{-1}) at the 3.6 m telescope, respectively. After our independent discovery of the afterglow, second-epoch observations plus some exposures with additional filters were obtained ($\sim$4 hr later) at the end of that night. Multicolor photometry continued at the NTT and 3.6 m telescope during the next 3 days and at the VLT thereafter. Because of the rapidly decreasing afterglow brightness, we switched to the instruments at the 8.2 m Very Large Telescope (VLT) starting on day 3 after the GRB. For our NIR observations the short-wavelength (0.9–2.5 μm) arm of the infrared spectrometer ISAAC (equipped with a 1024×1024 pixel Rockwell HgCdTe array and a plate scale of $0\farcs147$ pixel^{-1}) on the VLT telescope Antu was used, and for the optical observations the Focal Reducer and Spectrograph (FORS; equipped with an SITe CCD with 24 μm pixels and a plate scale of $0\farcs2$ pixel^{-1}) at VLT/Yepun was used.

Additional imaging was performed in the R and I bands at the ESO 1.54 m Danish telescope on La Silla (Chile), in the H band at the Anglo-Australian Telescope (AAT), and in the J and H bands at the 4 m Blanco telescope of the Cerro Tololo Inter-American Observatory (CTIO). The 1.54 m Danish telescope was equipped with a 2048×4096 EEV/MAT frame-transfer CCD (illuminated area is 2048×2048 pixel) with 15 μm pixels, which provides a plate scale of $0\farcs39$ pixel^{-1}. At the AAT the IRIS2 instrument with a 1024×1024 Rockwell HAWAII-1 HgCdTe detector was used, having a pixel scale of $0\farcs446$ pixel^{-1}. At CTIO, the Ohio State Infrared Imager/Spectrometer (OSIRIS) with a 1024×1024 HAWAII-1 HgCdTe detector was used, having a plate scale of $0\farcs161$ pixel^{-1}.

2.3. *Spectroscopy*

Spectroscopic observations were performed during the first 2 days in several wavelength bands to derive the redshift and during the maximum of the late-time bump to search for signatures of the potential SN and to derive host galaxy parameters. In the JK bands the short-wavelength arm of ISAAC was used at low resolution (with a final dispersion of 3.6 Å pixel^{-1} in the J band and 7.2 Å pixel^{-1} in the K band); the $1\farcs0$ slit was used. The J- and K-band spectra were both taken at $1\farcs2$ seeing, thus giving an FWHM resolution of 29 (J band) and 59 Å (K band).

Optical spectra were taken with FORS2 at the Yepun telescope at three different occasions, each with a different grism (see Table 1). The 150I grism has a mean 5.5 Å pixel^{-1} scale, which at the $0\farcs5$ seeing and with the use of a $0\farcs7$ slit led to a resolution of 14 Å (FWHM). Grism 300I has a mean 2.59 Å pixel^{-1} scale, leading to a resolution of 13 Å (FWHM) at $0\farcs7$–$1\farcs2$ seeing and use of the $1\farcs0$ slit. Finally, grism 600B with a mean 1.2 Å pixel^{-1} scale at $1\farcs2$–$1\farcs5$ seeing and the $1\farcs0$ slit led to an FWHM resolution of 6 Å. The pixel scale changes by less than 5% from the red to the blue end of each grism. The peak spectral response for the 150I, 300I, and 600B grism is at 5000, 7500, and 4000 Å, respectively.

3. DATA REDUCTION, ANALYSIS, AND BASIC RESULTS

3.1. *Photometry*

The optical and near-infrared images were reduced in standard fashion using IRAF,[22] as well as ESO's *eclipse* package (Devillard 2002[23]). Photometric calibration of the GRB field was performed using SExtractor (Bertin & Arnouts 1996). Air-mass correction was done according to the coefficients provided by ESO's Web sites (in units of mag per air mass): $k_B = 0.240 \pm 0.007$, $k_V = 0.112 \pm 0.005$, $k_R = 0.091 \pm 0.007$, $k_I = 0.061 \pm 0.006$ for VLT FORS1 and FORS2, and $k_J = 0.06$, $k_H = 0.06$, $k_K = 0.07$ for VLT ISAAC at Paranal, $k_B = 0.20$, $k_V = 0.11$, $k_R = 0.05$, $k_I = 0.02$ for La Silla. For the optical observations, the Landolt standard fields observed were SA 92-249, MarkA, Rubin 152, GD 108, and SA 100. For the NIR calibration the UKIRT infrared standard star FS 12 was used.

Local photometric standards (Tables 2, 3, 4) were selected according to their detection in $BVRI$ by SExtractor and a small scatter in their measured magnitudes on the images taken at different observing epochs. Moreover, care was taken that the difference between the deduced Bessel R-band magnitudes (FORS1) and the R_{special} magnitudes (FORS2) of these stars was less than about 0.1 mag. These local photometric standards were then used to derive the magnitude of the optical transient (Table 1) after removal of the host galaxy.

The accuracy of the photometry in the different filters has been cross-checked on the set of images taken on 2001 November 24 via a comparison of the observed stellar

[22] IRAF is distributed by the National Optical Astronomical Observatory, which is operated by the Associated Universities for Research in Astronomy, Inc., under contract to the National Science Foundation.

[23] Available at http://www.eso.org/projects/aot/eclipse/eug/eug/eug.html.

TABLE 1

LOG OF THE OBSERVATIONS

Date (UT)	Telescope/Instrument	Filter/Grism[a]	Exposure (s)	Seeing (arcsec)	Brightness[b] (mag)
2001 Nov 22 03:03–03:25.....	ESO NTT/SOFI	K_s	10×63	0.7	15.19 ± 0.07
2001 Nov 22 04:03–04:14.....	ESO 3.6 m/EFOSC2	R_C	3×180	1.5	18.86 ± 0.02
2001 Nov 22 07:30–08:01.....	ESO 3.6 m/EFOSC2	R_C	3×600	1.0	19.51 ± 0.01
2001 Nov 22 07:47–08:22.....	ESO NTT/SOFI	J	25×70	0.8	17.47 ± 0.04
2001 Nov 22 08:23–08:47.....	ESO NTT/SOFI	H	17×70	0.7	16.72 ± 0.05
2001 Nov 22 08:47–09:06.....	ESO NTT/SOFI	K_s	13×70	0.9	16.09 ± 0.07
2001 Nov 22 14:00–14:14.....	AAO AAT/IRIS2	H	10×60	2.7	17.30 ± 0.25
2001 Nov 23 00:04–00:20.....	ESO NTT/SOFI	K_s	11×70	1.2	17.71 ± 0.10
2001 Nov 23 00:20–00:39.....	ESO NTT/SOFI	J	13×70	1.6	19.38 ± 0.10
2001 Nov 23 04:30–04:40.....	ESO 3.6 m/EFOSC2	R_C	3×180	[c]	21.23 ± 0.05
2001 Nov 23 04:41–04:57.....	ESO 3.6 m/EFOSC2	B	3×300	[c]	22.40 ± 0.50
2001 Nov 23 04:58–05:08.....	ESO 3.6 m/EFOSC2	V	3×180	[c]	21.95 ± 0.15
2001 Nov 23 08:29–08:45.....	ESO NTT/SOFI	J	11×70	0.9	19.73 ± 0.10
2001 Nov 23 08:45–09:01.....	ESO NTT/SOFI	K_s	11×70	0.9	18.29 ± 0.10
2001 Nov 23 08:29–08:39.....	ESO 3.6 m/EFOSC2	R_C	3×180	1.3	21.75 ± 0.08
2001 Nov 23 08:39–08:44.....	ESO 3.6 m/EFOSC2	B	300	1.6	>21.70
2001 Nov 23 06:45–08:34.....	ESO Yepun/FORS2	600B	$2 \times 2400 + 1500$	1.5, 1.0, 1.2	...
2001 Nov 23 07:22–08:34.....	ESO Antu/ISAAC	1.1–1.4 μm	3600	1.2	...
2001 Nov 24 06:24–06:48.....	ESO Antu/ISAAC	K_s	15×60	0.7	19.30 ± 0.08
2001 Nov 24 06:53–07:16.....	ESO Antu/ISAAC	H	15×60	0.7	19.81 ± 0.05
2001 Nov 24 07:18–07:36.....	ESO Antu/ISAAC	J_s	10×90	0.6	20.93 ± 0.10
2001 Nov 24 07:53–08:59.....	ESO Antu/ISAAC	1.95–2.55 μm	3600	1.2	...
2001 Nov 24 07:43–08:01.....	ESO Yepun/FORS2	B	3×300	0.8	23.70 ± 0.30
2001 Nov 24 08:02–08:14.....	ESO Yepun/FORS2	V	3×180	0.8	23.37 ± 0.05
2001 Nov 24 08:15–08:27.....	ESO Yepun/FORS2	$R_{special}$	3×180	0.8	22.93 ± 0.08
2001 Nov 25 06:43–06:59.....	ESO Antu/ISAAC	J_s	10×90	0.9	21.64 ± 0.30
2001 Nov 25 07:01–07:24.....	ESO Antu/ISAAC	H	15×60	0.6	20.73 ± 0.10
2001 Nov 25 07:27–07:52.....	ESO Antu/ISAAC	K_s	15×60	0.8	20.02 ± 0.10
2001 Nov 25 06:34–08:10.....	ESO Yepun/FORS2	150I	3×1800	0.5	...
2001 Nov 25 08:10–08:22.....	ESO Yepun/FORS2	$R_{special}$	3×180	0.8	23.68 ± 0.15
2001 Nov 25 08:23–08:34.....	ESO Yepun/FORS2	V	3×180	[d]	>24.40
2001 Nov 25 07:41–08:13.....	ESO 1.54 m Danish	R_C	1880	1.1	23.60 ± 0.40
2001 Nov 30 08:05–08:51.....	CTIO OSIRIS	H	19×60	0.7	>19.40
2001 Dec 01 08:07–08:39	CTIO OSIRIS	J	8×120	0.9	>20.10
2001 Dec 03 07:50–08:25	CTIO OSIRIS	J	10×120	1.2	>20.10
2001 Dec 05 06:28–07:01	ESO Melipal/FORS1	V	3×600	0.9	24.30 ± 0.02
2001 Dec 05 07:02–07:33	ESO Melipal/FORS1	R_C	3×600	0.9	23.20 ± 0.08
2001 Dec 05 07:34–08:07	ESO Melipal/FORS1	I_C	3×600	0.9	22.35 ± 0.25
2001 Dec 05 06:53–08:09	ESO Antu/ISAAC	J_s	40×90	0.6	22.41 ± 0.15
2001 Dec 07 06:45–08:02	ESO Antu/ISAAC	J_s	40×90	0.6	22.69 ± 0.10
2001 Dec 08 06:20–06:30	ESO Melipal/FORS1	V	600	0.8	24.09 ± 0.02
2001 Dec 09 06:49–08:05	ESO Antu/ISAAC	J_s	40×90	0.7	22.52 ± 0.15
2001 Dec 09 07:33–07:43	ESO Melipal/FORS1	V	600	1.0	23.94 ± 0.02
2001 Dec 10 06:47–06:57	ESO Melipal/FORS1	R_C	600	0.8	23.65 ± 0.08
2001 Dec 11 07:33–08:06	ESO Melipal/FORS1	R_C	3×600	0.6	23.45 ± 0.08
2001 Dec 11 08:07–08:29	ESO Melipal/FORS1	V	2×600	0.7	24.18 ± 0.02
2001 Dec 12 05:12–07:30	ESO Yepun/FORS2	300I	4×1800	0.7–1.2	...
2001 Dec 13 07:19–08:46	ESO Antu/ISAAC	J_s	40×90	0.7	22.89 ± 0.15
2001 Dec 15 05:10–05:27	ESO 1.54 m Danish	I_C	4×900	1.2	>24.70
2001 Dec 16 04:51–05:08	ESO 1.54 m Danish	I_C	2×900	1.3	>23.90
2001 Dec 17 04:55–05:12	ESO 1.54 m Danish	I_C	4×900	2.0	>23.80
2001 Dec 17 07:20–08:47	ESO Antu/ISAAC	J_s	40×90	1.0	22.79 ± 0.30
2001 Dec 18 04:45–05:01	ESO 1.54 m Danish	I_C	2×900	1.1	>23.80
2002 Feb 09 04:04–05:24	ESO Antu/ISAAC	J_s	40×90	0.5	>24.85

[a] The $R_{special}$ filter is about 10% broader than the standard R_C. Filters J_s and K_s are narrower with respect to the canonical J and K bands, respectively: J_s has a width of 0.16 μm (instead of 0.29 μm), and K_s has a width of 0.29 μm centered at 2.16 μm (instead of 0.35 μm centered at 2.20 μm). However, since both narrowband filters have a higher transmission than the canonical filters, the net effect is that $J-J_s \lesssim 0.05$ ($K-K_s \lesssim 0.02$) when comparing the ISAAC J_s vs. the SOFI J filter. The grisms 150I, 300I, and 600B are described in the text.

[b] Not corrected for Galactic foreground extinction.

[c] Image quality affected by guiding problems.

[d] Variable seeing due to varying cirrus.

TABLE 2
LOCAL PHOTOMETRIC B, V STANDARDS

Star	R.A. (J2000.0)	Decl. (J2000.0)	B	V
B1	11 34 18.9	−76 01 37	20.11 ± 0.01	18.93 ± 0.01
B2	11 34 19.7	−76 02 06	20.95 ± 0.01	19.95 ± 0.02
B3	11 34 27.2	−76 01 52	22.93 ± 0.03	21.93 ± 0.04
B4	11 34 27.2	−76 02 34	23.94 ± 0.07	22.49 ± 0.05
B5	11 34 27.4	−76 02 22	21.58 ± 0.01	20.35 ± 0.02
B6	11 34 29.9	−76 02 36	23.69 ± 0.05	22.27 ± 0.05
B7	11 34 33.3	−76 01 33	20.64 ± 0.01	19.59 ± 0.01
B8	11 34 36.2	−76 01 07	23.00 ± 0.05	21.41 ± 0.04
B9	11 34 38.9	−76 01 38	20.37 ± 0.01	19.03 ± 0.01
B10	11 34 41.9	−76 01 04	25.25 ± 0.16	23.01 ± 0.09
B11	11 34 52.9	−76 01 31	23.50 ± 0.05	21.57 ± 0.03

NOTES.—Units of right ascension are hours, minutes, and seconds, and units of declination are degrees, arcminutes, and arcseconds. B4 = R5, B6 = R6, B7 = J2.

brightnesses versus those of expected synthetic stars. For this we have first measured the magnitudes of our local standard stars using YODA (Drory 2003), after having convolved the images to the common worst seeing of 1.″4. In a second step, we took synthetic stellar spectra from the Pickles spectral library and convolved those with the filter transmission curves and efficiencies of the corresponding instrument (FORS2+ISAAC). Finally, we overplotted the measured standards over the synthetic stars in various color-color diagrams (Fig. 3). This shows that the photometric calibration is of coherent quality over all seven filter bands used.

3.2. *The Light Curve*

GRB 011121 occurred at Galactic coordinates $(l, b) = (297.^{\circ}77, -12.^{\circ}43)$. The Schlegel, Finkbeiner, & Davis (1998) extinction maps predict $E(B-V) = 0.46$ mag along this line of sight through the Galaxy. Assuming the usual ratio of visual to selective extinction of 3.1, this gives $A_V \approx 1.4$ mag. The H I maps of Dickey & Lockman (1990) give $N_{\rm H} = 1.2 \times 10^{21}$ cm^{-2}, which translates into $A_V \approx 0.9$ mag using the extinction-to-absorption correlation of Predehl & Schmitt (1995). We used the higher of the above two values and then followed standard procedures (Rieke & Lebofsky 1985; Cardelli, Clayton, & Mathis 1989; Reichart 2001) to calculate the extinction in the other photometric bands, resulting in $A_B = 1.87$ mag, $A_{R_{\rm C}} = 1.15$ mag, $A_{I_{\rm C}} = 0.83$ mag, $A_J = 0.40$ mag, $A_H = 0.25$ mag, and $A_{K_s} = 0.17$ mag. In all the light-curve plots this extinction has been corrected for.

TABLE 3
LOCAL PHOTOMETRIC $R_{\rm C}$, $I_{\rm C}$ STANDARDS

Star	R.A. (J2000.0)	Decl. (J2000.0)	$R_{\rm C}$	$I_{\rm C}$
R1.....	11 34 10.8	−76 02 50	20.87 ± 0.05	20.06 ± 0.02
R2.....	11 34 11.2	−76 03 23	20.96 ± 0.02	20.35 ± 0.02
R3.....	11 34 15.4	−76 00 37	19.97 ± 0.04	19.34 ± 0.01
R4.....	11 34 18.0	−76 02 32	23.43 ± 0.10	22.95 ± 0.08
R5.....	11 34 27.2	−76 02 34	21.75 ± 0.04	21.09 ± 0.03
R6.....	11 34 29.9	−76 02 36	21.48 ± 0.04	20.80 ± 0.03
R7.....	11 34 33.3	−76 02 30	21.82 ± 0.06	21.13 ± 0.03
R8.....	11 34 40.8	−76 02 36	20.47 ± 0.03	19.98 ± 0.01
R9.....	11 34 41.9	−76 01 35	22.36 ± 0.05	21.84 ± 0.05
R10.....	11 34 43.8	−76 01 27	22.78 ± 0.07	21.49 ± 0.04
R11.....	11 34 45.4	−76 01 32	19.36 ± 0.08	18.87 ± 0.01

NOTES.—Units of right ascension are hours, minutes, and seconds, and units of declination are degrees, arcminutes, and arcseconds. R5 = B4, R6 = B6.

Accurate photometry of the afterglow requires a careful removal of contaminating light from the underlying GRB host galaxy, which has an angular extent of 2″ (Fig. 4). This was accomplished with a two-component intensity profile model, as described in more detail in § 4.4. The model is derived from the J-band image of 2002 February 9, taken at a seeing of 0.″45. We assume that the radial profile of the host galaxy is the same in all filter bands, as justified by a comparison of the scale lengths of 86 face-on galaxies in the B, V, R, and H filter bands by de Jong (1996), who finds that they are identical within the errors (the disk scale length ratio of R vs. H band is 1.07 ± 0.08). The subtraction is done in count space on the images before the photometry, and for each image the host model is first convolved with the seeing of that exposure and then iteratively adjusted in intensity until the area around the afterglow is best matched to the undisturbed background somewhat farther away. As a consistency test we computed the host magnitude for each image, taking into account the seeing convolution and the final intensity normalization, and found that the host magnitude differs at most by 0.07 mag (two instances) from the values given in § 4.4. In addition, star 1 from Figure 5 has been used to monitor the quality of the subtraction, which was always accurate to better than 0.05 mag. This ensures that the light-curve shape is not contaminated by this subtraction procedure. An example of the result is shown in Figure 6.

3.2.1. *Light Curve Based on Observations prior to $t = 10$ days*

Figure 7 shows the afterglow light curve in the $R_{\rm C}$ band after removal of the flux from the underlying host galaxy and after correcting for Galactic extinction. Theoretical fits were obtained with the formula of Beuermann et al. (1999) in the representation of Rhoads & Fruchter (2001):

$$F_\nu(t) = 2^{1/n} F_\nu(t_b) \left[\left(\frac{t}{t_b} \right)^{\alpha_1 n} + \left(\frac{t}{t_b} \right)^{\alpha_2 n} \right]^{-1/n} . \qquad (1)$$

Here F_ν is the flux density, t_b is the break time (in days), and n is the parameter that describes the smoothness of the break. In all cases we fitted apparent magnitudes. Here and in the following we use the standard notation for the time and frequency dependence of the flux density in the simple fireball model: $F_\nu \propto t^{-\alpha} \nu^{-\beta}$.

The fit of the $R_{\rm C}$-band data excluding the measurements at $t \geq 10$ days gives an early-time slope of $\alpha_1 = 1.62 \pm 0.62$, a late-time slope of $\alpha_2 = 2.44 \pm 0.38$, and a break time of $t_b = 1.2 \pm 1.0$ days ($\chi^2/{\rm dof} = 0.45$, where dof stands for degrees of freedom). The parameter n, which measures the sharpness of the break, was fixed at $n = 10$, corresponding to a sharp break. However, values as low as $n = 1$ give similarly good fits.

At early times (2001 November 22, 3:30 UT) we measure $R_{\rm C}-K = 2.7 \pm 0.1$ mag (after correction for Galactic extinction). Hence, the spectral slope of the afterglow is $\beta = 0.80 \pm 0.15$. Two days later, on 2001 November 24, 7:00 UT, we find $\beta = 0.62 \pm 0.05$ based on our $BVRJHK$

TABLE 4

LOCAL PHOTOMETRIC STANDARDS FOR THE NIR BANDS (FIG. 5)

Star	R.A. (J2000.0)	Decl. (J2000.0)	J_s	H	K_s
J1	11 34 39.0	−76 01 17	15.21 ± 0.05	14.81 ± 0.05	14.91 ± 0.05
J2	11 34 33.3	−76 01 33	17.28 ± 0.05	16.74 ± 0.05	16.82 ± 0.05
J3	11 34 25.8	−76 01 37	18.56 ± 0.05	18.28 ± 0.05	18.27 ± 0.05
J4	11 34 35.6	−76 01 53	17.15 ± 0.05	16.31 ± 0.05	16.31 ± 0.05

NOTE.—Units of right ascension are hours, minutes, and seconds, and units of declination are degrees, arcminutes, and arcseconds.

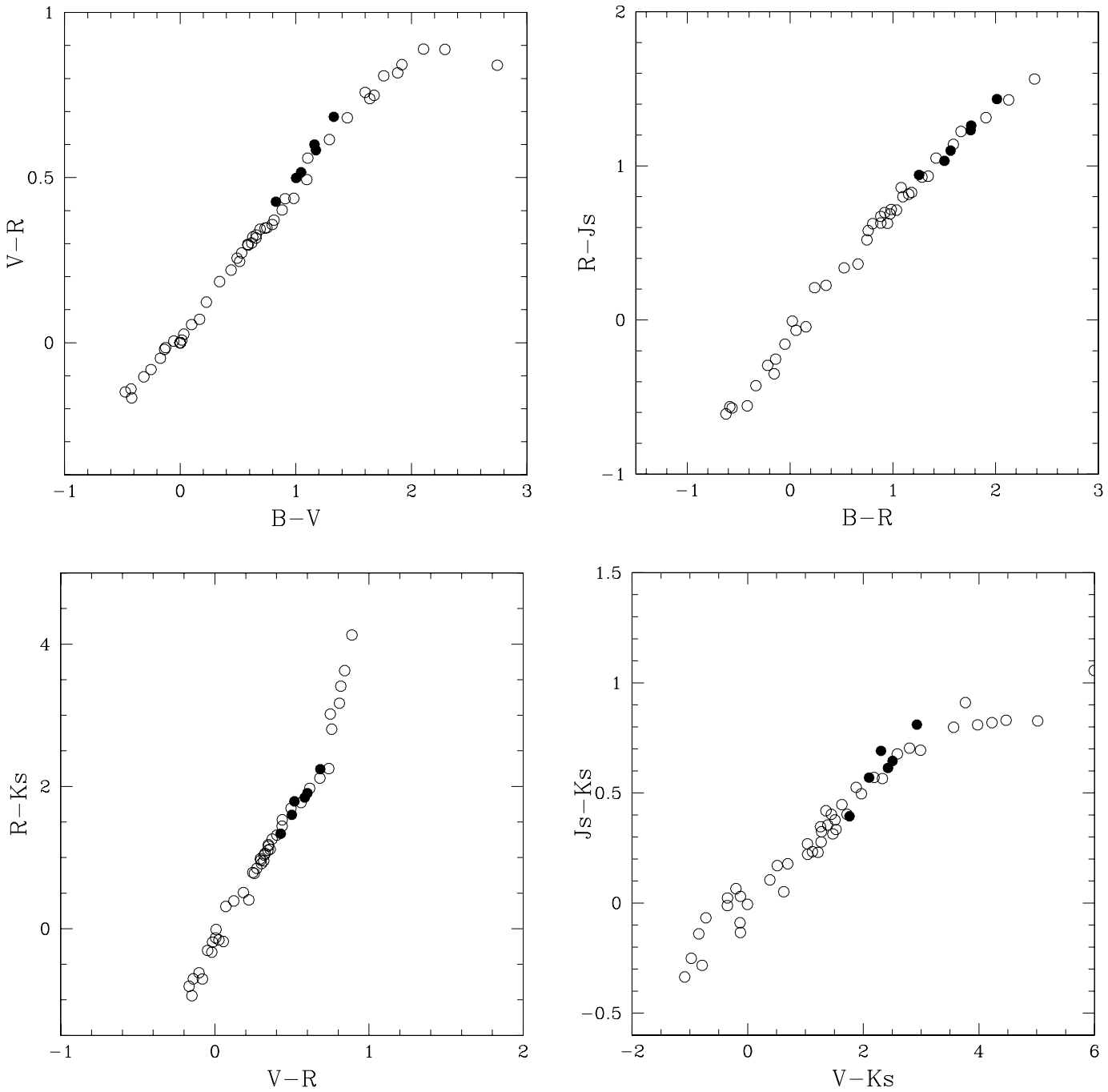

FIG. 3.—Color-color diagrams of bright, nonsaturated stars detected in the central area of the images of GRB 011121 (*filled circles*), compared with the expected color-color sequence as derived from the convolution of the stellar library of Pickles with the total filter efficiency curves of the instruments used (*open circles*).

FIG. 4.—Sequence of *J*-band images of GRB 011121 taken with SOFI/NTT on 2001 November 22 (*left*) and with VLT/ISAAC on 2001 November 24 (*middle*) and 2002 February 9 (*right*). The rightmost image clearly shows the host galaxy (labeled 3 in Fig. 5), whereas the GRB afterglow has disappeared. The field is $17'' \times 17''$. North is at the top and east to the left. [*See the electronic edition of the Journal for a color version of this figure*.]

data, which is consistent with the earlier result and is fully in agreement with the results obtained by Garnavich et al. (2003) and Price et al. (2002). These afterglow parameters are fully consistent with those expected from the simple versions of the fireball, as well as observations of previous GRB afterglows (e.g., van Paradijs, Kouveliotou, & Wijers 2000).

We can improve the fit by adding more data points as follows. First, using the deduced spectral index of the early afterglow, we can estimate that at the time of the single AAO observations (Table 1), i.e., before the deduced break time, the R_C-band magnitude of the optical transient was 20.12 ± 0.25. Second, we can include in our fit the *R*-band data from Garnavich et al. (2003) for $t < 0.6$ days. In doing so, we get $\alpha_1 = 1.62 \pm 0.39$, $\alpha_2 = 2.44 \pm 0.34$, $t_b = 1.20 \pm 0.75$ days, and $\chi^2/\mathrm{dof} = 1.11$.

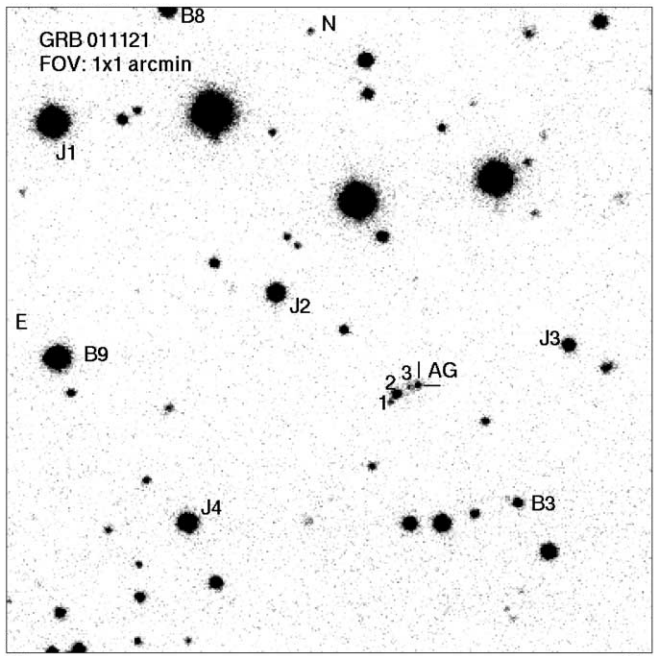

FIG. 5.—*J*-band finding chart of GRB 011121 obtained on 2001 November 24 with ISAAC/VLT. Marked are the afterglow (AG), neighboring objects (1, 2), the host galaxy (3), and some local standards (J1–J4, B3, B8, B9).

3.2.2. *Light Curve Based on All Observations*

Including the "late-time" data (after $t = 10$ days) to the fits adds substantially more freedom, since different model components can now compensate each other. As before, we only use R_C-band data for the analysis. In order to account for the excess light after $t = 10$ days, we assume that this "bump" is due to light from an underlying SN. In fact, it has been officially designated as SN 2001ke (Garnavich et al. 2003). To model this SN component, we employ the observed $UBVR_CI_C$ light curves of SN 1998bw (Galama et al. 1998) as a template.

The effects of the redshift of GRB 011121 ($z = 0.36$) were taken into account assuming the cosmological parameters as given in § 2.1. For SN 1998bw we used a redshift of $z = 0.0085$ (Tinney et al. 1998). The entire numerical procedure is explained in detail in Zeh & Klose (2003). It interpolates smoothly between the *UBVRI* light curves of SN 1998bw (Galama et al. 1998),[24] so that for any given time a set of flux densities is calculated. The predicted time-dependent SN light curve of a redshifted GRB SN based on the SN 1998bw template is then calculated according to the procedure outlined by Dado, Dar, & De Rujula (2002a). The apparent magnitude of a redshifted SN 1998bw in a given photometric band is finally obtained by integrating over the flux densities (transformed into per unit wavelength), multiplied by the corresponding filter response function, and by applying the usual normalization factors. The entire procedure has been successfully applied for GRB 030329/SN 2003dh (Hjorth et al. 2003; Zeh et al. 2003) and has been successfully tested against the results obtained by others for other bursts (e.g., Masetti et al. 2003; Dado et al. 2002a). The results are shown in Figures 8 and 9.

The resulting parameters are $\alpha_1 = 1.63 \pm 0.61$, $\alpha_2 = 2.73 \pm 0.45$, $t_b = 1.26 \pm 0.94$ days, and $k = 0.85 \pm 0.11$ with $\chi^2/\mathrm{dof} = 1.11$. Here k is the luminosity ratio in the R_C band between the GRB 011121 SN and SN 1998bw at maximum (at $z = 0.36$). As before, the parameter n was held

[24] See also http://zon.wins.uva.nl/~titus/grb980425.html.

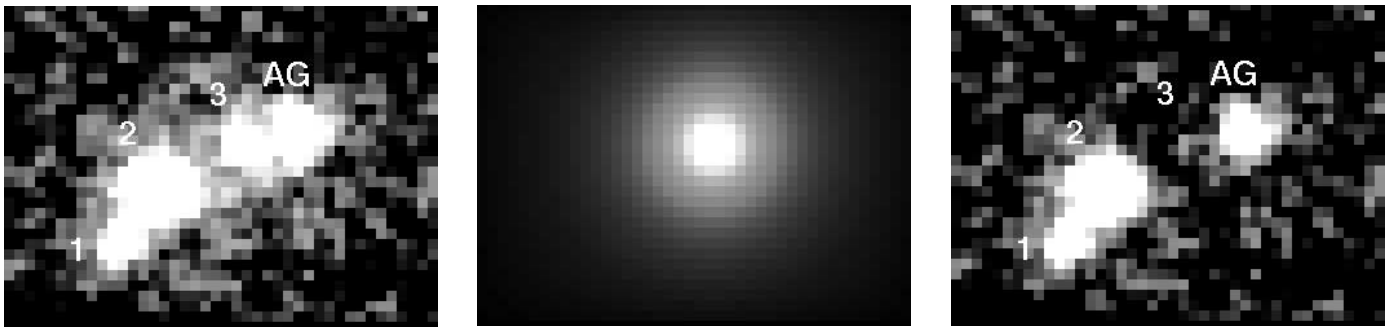

FIG. 6.—Sequence of *R*-band subimages of 2001 November 24 showing the original (*left*), the model of the host galaxy (*middle*), and the host-subtracted image (*right*). All subimages are shown at the same scale and with the same cut values. Labels are the same as in Fig. 5. Photometry of the lower left star in the original and the host-subtracted image has been done for all epochs to ensure that no oversubtraction occurred. The residual scatter in this comparison star was in the range of 0.02–0.05 mag. [*See the electronic edition of the Journal for a color version of this figure.*]

constant at 10 because otherwise the sparse data would not allow convergence of the numerical fitting algorithm. Our conclusions are not sensitive to the exact value of this parameter. On the other hand, we emphasize that the value we get for the parameter k assumes a "perfect" SN 1998bw light curve at the redshift of the burster. Any potential relation between luminosity and light-curve shape of an SN in a certain photometric band is neglected here. In particular, k does not say anything about the bolometric luminosity of the GRB SN compared to SN 1998bw. This parameter is also sensitive to potential additional parameters that one can introduce in order to improve the fit of the SN light curve (see § 4.2.2).

For SN 1998bw we assumed zero extinction along the line of sight through our Galaxy. Accordingly, our results obtained for the luminosity of the SN accompanying GRB 011121 in units of the luminosity of SN 1998bw, the parameter k, scale as $k \rightarrow k \exp[-A_V(\mathrm{SN\ 1998bw})/1.086]$, if such an extinction is taken into account. Note also that we assumed a Galactic extinction along the line of sight of $A_V(\mathrm{Gal}) = 1.4$ mag. If smaller values are preferred (Bloom et al. 2002b), k has to be corrected/reduced again.

Figures 4 (*middle panel*), 8, and 9 show that the SN light already affected the afterglow light a few days after the GRB. This implies a substantial impact on the measurement of the parameter α_2. Unfortunately, because of instrumental constraints, we have a data gap between days 4 and 10 after the burst trigger so that the 1 σ error of the deduced α_2 rises substantially when we include the SN light in the fit. Note that most of the data published previously are not host subtracted and therefore cannot be simply added to our data set (Brown et al. 2001; Phillips et al. 2001; Price et al. 2001; Stanek & Wyrzykowski 2001). Despite this added uncertainty, our analysis clearly indicates the presence of a break about 1 day after the burst. The exact time of the break is sensitive to the details of the fit (compare the results we obtain by fitting data prior to $t = 10$ days vs. fitting all the data), but the existence of the break at $t \sim 1$ day is clearly established. Previous studies of the afterglow light curve of GRB 011121 did not find this break (e.g., Price et al. 2002;

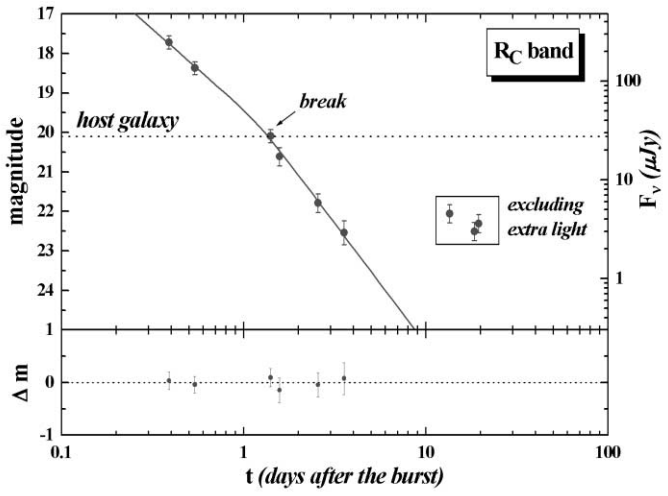

FIG. 7.—R_C-band light curve of the afterglow of GRB 011121 and a fit to the data prior to $t = 10$ days. Compared to Table 1 a conservative systematic 1 σ error of 0.15 mag has been added to all data. The break in the power-law decay occurs at $t_b = 1.2$ days. At late times the afterglow is significantly brighter than predicted by the power law. Note the particularly bright host galaxy. [*See the electronic edition of the Journal for a color version of this figure.*]

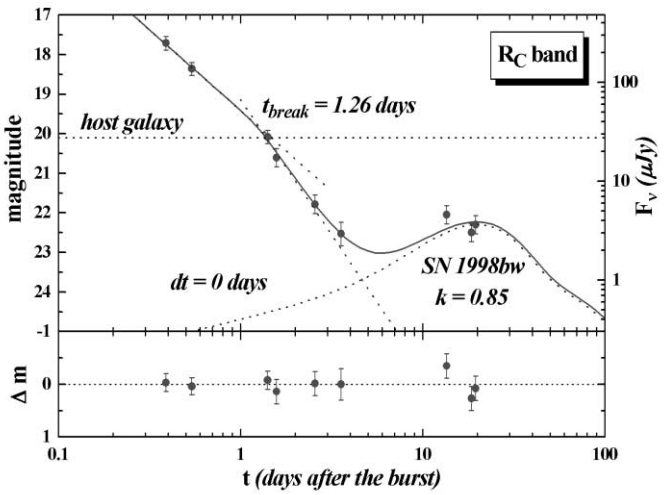

FIG. 8.—R_C-band light curve based on eq. (1) and an additional SN component, assuming $dt = 0$ days (eq. [2]). Note that all photometric data are corrected for Galactic extinction (§ 3.2). Compared to Table 1 a conservative systematic 1 σ error of 0.15 mag has been added to all data. [*See the electronic edition of the Journal for a color version of this figure.*]

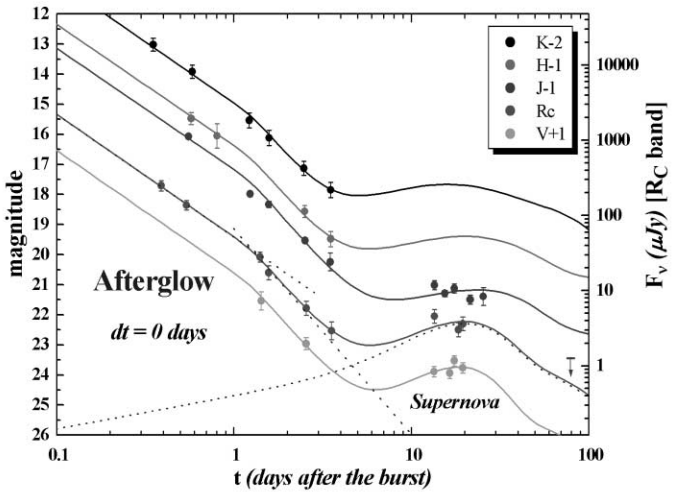

FIG. 9.—Same as Fig. 8, but now showing the best fit in all photometric bands. When fitting the *V*-, *J*-, *H*-, and K_s-band light curves, the afterglow parameters deduced from the R_C-band fit (α_1, α_2, [*n*], t_b) were used as input; i.e., the functional form of the afterglow light curve was fixed. The SN light curve (extrapolated toward the *H* and *K* bands), however, was calculated for the chosen photometric band. [*See the electronic edition of the Journal for a color version of this figure*.]

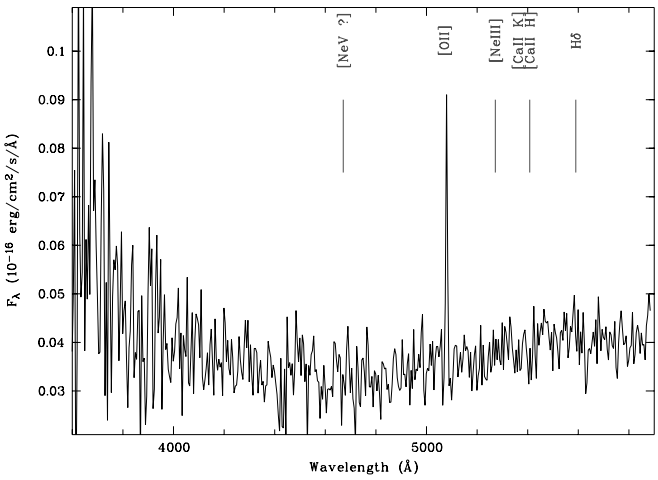

FIG. 10.—Spectrum of GRB 011121 in the blue band, taken on 2001 November 23 with VLT/FORS2 equipped with the 600B grism. While only the [O II] line is detected beyond doubt, we also indicate the positions of other lines that could have been expected. [*See the electronic edition of the Journal for a color version of this figure*.]

Garnavich et al. 2003), which can be attributed to sparse sampling of the afterglow at this particular time. It remains difficult to explain why the radio data of the afterglow do not agree with a jet model (Price et al. 2002).

3.3. *The Spectrum of the Afterglow*

The VLT/FORS2 spectrum of the afterglow (including light from the host galaxy and the underlying SN) contains several strong emission lines (Fig. 10, Table 5), but no absorption lines. The redshift determined from these lines is $z = 0.362 \pm 0.001$ (see the figures for line identifications), consistent with the results of Infante et al. (2001). This redshift corresponds to a luminosity distance of 2.07 Gpc (assuming the cosmological parameters of § 2.1) and a distance modulus of 41.59 mag.

Using the foreground A_V (§ 3.2), we have determined the extinction values in the lines, $A^{\rm line}$, and corrected the measured line fluxes according to $F_{\rm corr} = F_{\rm obs}\exp(\tau)$, where $\tau = 1/1.086A^{\rm line}$ is the continuum extinction according to the Galactic A_V.

4. RESULTS AND DISCUSSION

4.1. *The Afterglow Model and the α-β Relations*

Since our finding of a jetted explosion is crucial for an understanding of the observational data, we have carefully checked this result. When we fit our R_C-band data (Table 1) with a single power-law plus SN component, we get $\alpha = 1.98 \pm 0.11$, $k = 0.81 \pm 0.11$ with $\chi^2/{\rm dof} = 1.49$. Not only is the fit worse in comparison to the fit based on the Beuermann equation, but the value we now get for α is notably larger (3 σ deviation) than the one deduced for the early-time slope of the afterglow light curve (Price et al. 2002; Garnavich et al. 2003). This again points to a change in the fading behavior of the afterglow between about 0.4 and 2 days after the burst. Moreover, our deduced α_1 for the early-time slope of the afterglow light curve is fully consistent with the result obtained by Price et al. (2002) and Garnavich et al. (2003) based on their optical/NIR data. In fact, when we fit their data, we confirm that they do not show evidence for a break in the light curve. We attribute this to the lack of data around $t = 1$ day. This makes us confident that the break in the light curve that we deduce based on our observations is a real effect.

In Table 6 we list the predicted spectral slope β corresponding to the measured α-values for various afterglow

TABLE 5

MEASURED LINE FLUXES (CORRECTED FOR GALACTIC EXTINCTION) AND LUMINOSITIES

Line	$\lambda_{\rm obs}$ (Å)	z	Flux (10^{-16} ergs cm^{-2} s^{-1})	Luminosity (10^{40} ergs s^{-1})
[O II] λ3726	5079	0.363	0.41 ± 0.03	8.6
Hβ	6625	0.362	0.22 ± 0.04, 0.14 ± 0.04[a]	3.2, 2.0
[O III] λ4963	6760	0.362	0.11 ± 0.06, 0.08 ± 0.05[a]	1.6, 1.1
[O III] λ5007	6821	0.362	0.35 ± 0.05, 0.16 ± 0.04[a]	4.9, 2.2
Hα	8945	0.363	0.96 ± 0.08, 0.81 ± 0.09[a]	9.2, 7.7
Paα	25550	0.362	2.58 ± 0.12	14.8

[a] The first number is measured from the 150I spectrum on 2001 November 25, while the second number is measured from the 300I spectrum on 2001 December 12.

TABLE 6
PREDICTED β-VALUES FOR VARIOUS AFTERGLOW SCENARIOS

Afterglow Model	$\beta(\alpha)$	Predicted β	Electron p
ISM, ISO, case 1.....	$(2\alpha+1)/3$	1.41 ± 0.26	2.82 ± 0.52
ISM, ISO, case 2.....	$2\alpha/3$	1.08 ± 0.26	3.16 ± 0.52
ISM, jet, case 1	$\alpha/2$	1.22 ± 0.17	2.44 ± 0.34
ISM, jet, case 2	$(\alpha-1)/2$	0.72 ± 0.17	2.44 ± 0.34
Wind, ISO, case 1	$(2\alpha+1)/3$	1.41 ± 0.26	2.82 ± 0.52
Wind, ISO, case 2	$(2\alpha-1)/3$	0.75 ± 0.26	2.50 ± 0.52
Wind, jet, case 1	$\alpha/2$	1.22 ± 0.17	2.44 ± 0.34
Wind, jet, case 2	$(\alpha-1)/2$	0.72 ± 0.17	2.44 ± 0.34

NOTES.—Assuming a relativistic jetted explosion then for observations at $t < t_{\rm break}$ (prebreak time), the isotropic model holds and $\alpha = \alpha_1$, whereas for $t > t_{\rm break}$ (postbreak time) the jet model applies and $\alpha = \alpha_2$. We use here $\alpha_1 = 1.62 \pm 0.39$ and $\alpha_2 = 2.44 \pm 0.34$ (see § 3.2.1). The parameter s is the power-law index of the density profile of the circumburst medium, $n(r) \propto r^{-s}$. For an ISM model $s = 0$, for a wind model $s = 2$. Case 1 stands for $\nu > \nu_c$, case 2 for $\nu < \nu_c$. In the former case the electron power-law index is given by $p = 2\beta$, whereas in the latter case $p = 2\beta + 1$ (e.g., Sari et al. 1999).

scenarios. Basically, we have to decide here between an interstellar medium (ISM) and a wind model for a jetted explosion and to constrain the position of the cooling break frequency in the spectral energy distribution (SED) of the afterglow light at the time of the observation. From the comparisons of the predicted β, based on the theoretical α-β relations, with the observed one on 2001 November 22, 3:30 UT, and on 2001 November 24, 7:00 UT, we conclude as follows (see also Fig. 11):

1. The model predictions agree best with the observations for the wind scenario. In this model, the presence of a late "bump" is the natural consequence of the SN following the stage of rapid mass loss in a massive progenitor star.

2. The data favor the interpretation that during our observations the cooling break frequency ν_c, which separates the contribution of fast-cooling electrons from slow-cooling electrons in the afterglow light (see Sari, Piran, & Narayan 1998 for their original definition), was above the optical/NIR bands ($\nu_c \gtrsim 10^{15}$ Hz). This is in agreement with the conclusions drawn by Price et al. (2002) based on their observational data; we refer the reader to this publication for a further discussion of this point.

3. The power-law index p of the electron energy distribution, $N(\gamma_e)d\gamma_e \propto \gamma_e^{-p}\, d\gamma_e$, was close to the expectations from particle acceleration in relativistic shocks (e.g., Sari, Piran, & Halpern 1999).

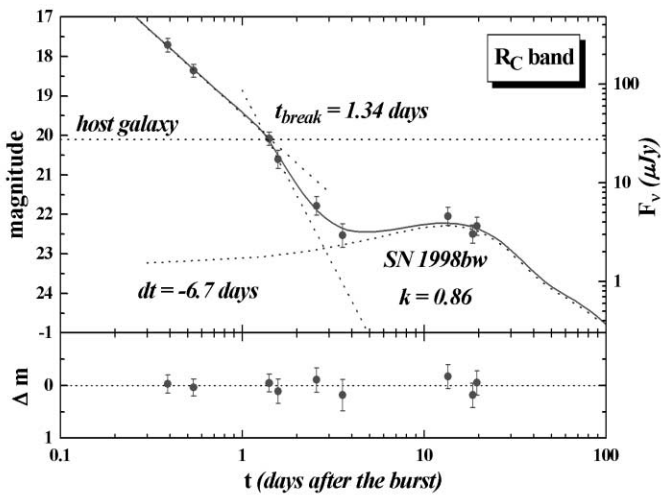

FIG. 11.—Same as Fig. 8, but with dt (eq. [2]) as a further free parameter. [*See the electronic edition of the Journal for a color version of this figure.*]

Within our measurement errors, there is no need for an additional extinction by dust in the GRB host galaxy. A wavelength-dependent extinction by cosmic dust in the GRB host galaxy would tend to increase β, i.e., redden the afterglow light. For example, this was observed in the optical/NIR afterglow of GRB 000418 (Klose et al. 2000). The low value of β we and others (Garnavich et al. 2003; Price et al. 2002) find for the afterglow of GRB 011121, however, after correction for the influence of reddening by Galactic dust, compared with various model predictions based on the observed light-curve shape (Table 6), gives us no strong hint for an additional dust component acting along the line of sight. Gray dust in the GRB host galaxy could still be there (wavelength-independent scattering cross section in the considered photometric bands), but this cannot be deduced from our data.

On the other hand, one should be aware of the fact that the results obtained are sensitive to the adopted Galactic extinction, A_V(Gal), along the line of sight. For example, if we had used $A_V(\mathrm{Gal}) = 0.9$ mag, as is suggested by the H I maps (§ 3.2), then the extinction-corrected β for the intrinsic optical afterglow would have been 1.1, based on our measured $R_C - K$ color of the optical transient on 2001 November 22, 3:30 UT. We favor the higher extinction value (1.4 mag), however. The early multicolor *UBVRIJK* observations of the GRB afterglow by Garnavich et al. (2003) give a best fit for the Galactic reddening along the line of sight of $E(B-V) = 0.43 \pm 0.07$ mag. For a standard ratio of total to selective extinction of 3.1, this is basically consistent with our chosen value for A_V(Gal). We note also that an adopted extinction of $A_V(\mathrm{Gal}) = 1.4$ mag is still consistent with the result deduced by Price et al. (2001) within their claimed 1 σ error bar [$A_V(\mathrm{Gal}) = 1.16 \pm 0.25$ mag].

We note that the observed change in the decay slope of the light curve around the break time is in agreement with the predictions of the jet-wind model, provided that the steepening of the light curve is due to the sideways expansion of the jet (Rhoads 1999).

It has been argued (Kumar & Panaitescu 2000) that for an external density profile as r^{-2} the jet break in the light curve is expected to be very gradual, taking at least two decades in time before most of the steepening sets in. In the case of GRB 011121, the break in the light curve is certainly shallower, extending no more than one decade in time (even with fits using $n = 1$ the "break" extends only from 0.5 to 2.5 days, still less than a decade). While this may be considered a problem, more extensive considerations have shown a large diversity of light-curve shapes, depending on not only the density profile but also the evolution of the Lorentz factor, whether jets are uniform or nonuniform, and the difference of viewing and jet angle (e.g., Wei & Jin 2003).

4.2. *The Supernova and the Wind Signature*

4.2.1. *Supernova Features*

The light curve of GRB 011121 provides the clearest case to date for excess emission above the usual power-law extrapolation. The excess in this case appears to become

significant about 1 week after the burst (Fig. 9). This feature has been heralded as strong evidence for an SN component (Bloom et al. 2002b; Dado, Dar, & De Rujula 2002b; Garnavich et al. 2003; Price et al. 2002). Garnavich et al. (2003) proposed the SN label SN 2001ke for this afterglow, although no obvious SN features were apparent in their Magellan/LDSS2 spectrum obtained on 2001 December 7. While it is far from proven that the late emission observed in GRB 011121 is in fact due to an SN, this interpretation is most natural. If we believe the SN bump picture, the observations of Garnavich et al. (2003) provide a stern warning: SN 1998bw (used in our analysis) may not be appropriate as a "template" for SN light associated with GRBs. Given that to date we have a rather limited sample of SNe associated with GRBs (see the recent review by Weiler et al. 2002), we are limited in what we can conclude from the bump in the afterglow of GRB 011121, except that it is obvious that the simple afterglow model is unable to explain features like these. Shock rejuvenation and inhomogeneities in the GRB environment or energy injection can explain the kind of bumpy afterglow observed in the case of GRB 021004 (e.g., Lazzati et al. 2002; Holland et al. 2003) but does not account for the long-term (weeks), sustained bump observed in GRB 011121. SNe, on the other hand, provide a natural explanation for the energy and also the timescale involved in the late bump we are considering here.

During the maximum of the SN bump (Fig. 12), the observed brightnesses of the afterglow are $J = 22.8 \pm 0.1$, $R = 23.4 \pm 0.1$, and $V = 22.8 \pm 0.1$. This is about 3.6, 3.3, and 3.7 mag fainter, respectively, than the total light of the host galaxy (see below). Although not all of the host was covered by the slit, the host galaxy still dominated the collected light, even for the spectrum taken on 2001 December 12, around the maximum of the bump. Thus, the lack of any SN signature in the spectrum is no argument against the SN

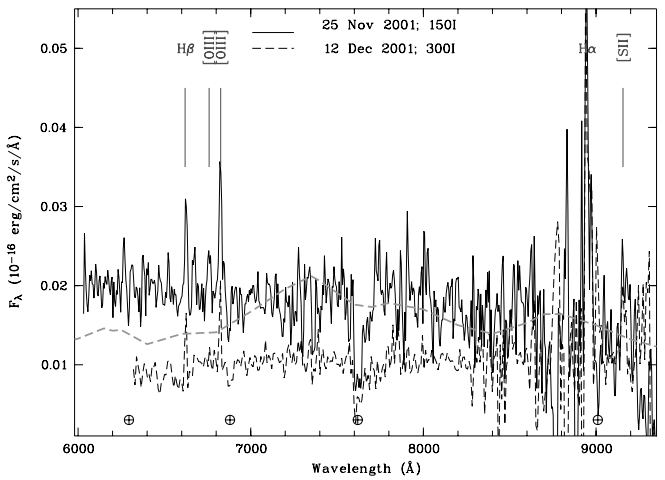

FIG. 12.—Spectrum of GRB 011121 in the red band, taken with VLT/FORS2 equipped with the 150I (2001 November 25; *top*) and 300I (2001 December 12; *bottom*; shifted by 0.01 units downward) grisms, respectively. Some line identifications are indicated. Taking slit losses on 2001 December 12 into consideration, both spectra represent basically the host spectrum, since at the covered wavelength range the afterglow has faded below the brightness of the host. The dashed line shows the spectrum of SN 1998bw 24 days after the maximum (Patat et al. 2001), redshifted to $z = 0.36$ and diminished in brightness to 85% (see § 3.2.2), thus clearly demonstrating that the SN was too faint with respect to the host galaxy to be discovered spectroscopically. [*See the electronic edition of the Journal for a color version of this figure.*]

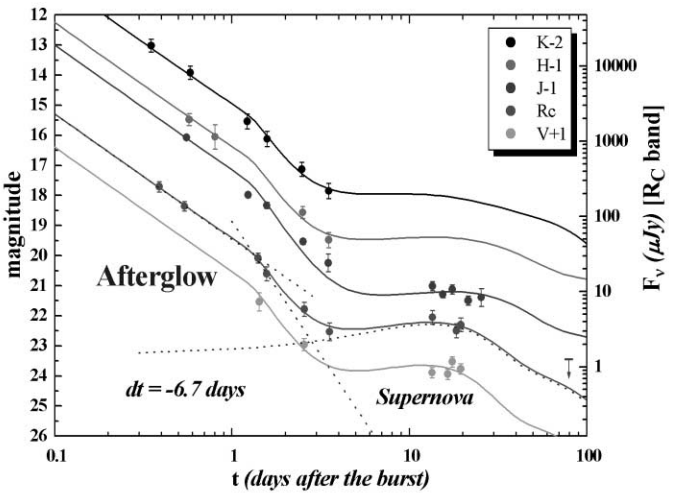

FIG. 13.—Same as Fig. 9, but for $dt = -6.7$ days. [*See the electronic edition of the Journal for a color version of this figure.*]

interpretation of the bump (Fig. 13), as pointed out by Garnavich et al. (2003).

The extinction-corrected (§ 3.2) absolute magnitudes for the SN with a *k*-correction in the *VRJ* bands of 0.85 mag (Leibundgut 1990), 0.55 mag, and zero, respectively, are $M_J = -19.18$, $M_R = -19.79$, and $M_V = -19.83$. Comparison with the absolute magnitudes of SN 1998bw suggests that the SN in GRB 011121 is slightly brighter in the *V* band but fainter at longer wavelengths.

4.2.2. *The GRB-Supernova Connection*

While we use SN 1998bw as a template SN, we added 1 dof to the fitting procedure by allowing for a shift *dt* of the observed SN maximum ($t^{\max}_{011121}$) with respect to the predicted one for a redshifted SN 1998bw ($t^{\max}_{1998bw}$), i.e.,

$$dt = t^{\max}_{011121} - t^{\max}_{1998bw} \, . \tag{2}$$

With this extra degree of freedom added, the best-fit parameters become $\alpha_1 = 1.67 \pm 0.58$, $\alpha_2 = 3.55 \pm 1.35$, $t_b = 1.34 \pm 0.60$ days, $k = 0.86 \pm 0.14$, and $dt = -6.7 \pm 5.2$ days with $\chi^2/\mathrm{dof} = 0.74$. As before, the parameter n was fixed at $n = 10$ (Figs. 12 and 14). The fact that α_2 is less well determined when we include the data points obtained after day 10 is not surprising. It is basically due to the lack of data between days 4 and 10 combined with the early and rapidly dominating SN component that makes the error of the deduced α_2 relatively large. This is also the reason why in Table 6, where we discuss the appropriate afterglow model, we used the fitting results obtained for those data when the SN component is still negligible.

The fit improves after inclusion of published late-time *Hubble Space Telescope* (*HST*) data (Bloom et al. 2002b). With these additional data we find for the *R*-band light curve $\alpha_1 = 1.66 \pm 0.44$, $\alpha_2 = 3.43 \pm 0.68$, $t_b = 1.33 \pm 0.48$ days, $k = 0.96 \pm 0.06$, and $dt = -5.1 \pm 1.85$ days with $\chi^2/\mathrm{dof} = 0.60$ (Fig. 15). Finally, if we follow § 3.2.1 and include the transformed *H*-band data point and the early-time data from Garnavich et al. (2003), we get basically the same result with slightly reduced error bars for α_1 and t_b.

It was already previously noted (Bloom et al. 2002b) that a negative time delay *dt* (eq. [2]) of order of a few days

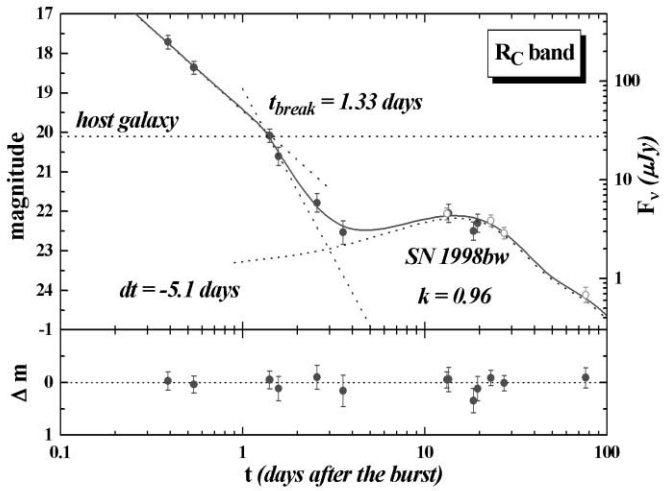

FIG. 14.—Same as Fig. 11, but with the inclusion of published *HST* *R*-band data from Bloom et al. (2002b). [*See the electronic edition of the Journal for a color version of this figure.*]

provides a better fit to the data than setting $dt = 0$ days, i.e., GRB and SN start at the same time. Basically, two scenarios could explain such a delay. First, this phenomenon could be intrinsic to the ejected SN shell itself in the sense that light-curve shapes of Type Ibc/II SNe are a function of the mass of the progenitor and other details of the explosion (as already remarked by Bloom et al. 2002b). The more exciting alternative is that this delay could point to a genuine time delay between the SN explosion (formation of a neutron star) and the GRB (interpreted as the subsequent formation of a black hole; see Vietri & Stella 1999). It is tempting to use the negative delay found in our fitting procedure as an argument in support of the supranova model (Vietri & Stella 1999).

However, it is worth remembering that the supranova model requires a delay between the SN and the GRB of many weeks to months (Vietri & Stella 1999), not days. If this delay is shortened, then the original goal of the model, namely, to explain the long-lived iron lines, is dismissed. Much better data on both the GRB afterglow and the SN light curve are required to establish the reality of such an offset. GRB 011121 has not been sampled enough to allow rigorous statements about the temporal relationship between SN and GRB, and the use of SN1998bw as a template is also a rather unreliable assumption of our modeling, as pointed out above and further discussed below.

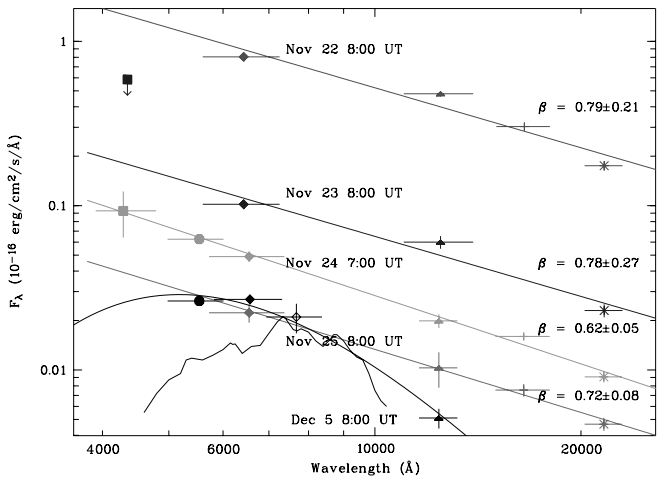

FIG. 15.—Extinction-corrected, broadband SED of GRB 011121 on 4 consecutive days, starting about 14 hr after the GRB, and on 2001 December 5 near the maximum of the SN bump. The best-fit power-law slopes β are given at the right-hand side except for December 5. The maximum deviation of the data to the power law is $\sim$0.15 mag, justifying the systematic error added in the light-curve fitting procedure. It can be seen that the spectral slope does not change over the first 4 days, supporting the jet nature of the break seen in the light curve. The December 5 (*filled circles*) spectrum is clearly not of power-law type. The smooth solid curve is a blackbody with a temperature of 6300 K, while the thin solid line is the spectrum of SN 1998bw, redshifted to $z = 0.36$. Note that on November 24, approximately 1 day after the break, the value of β is well defined and within the error bars well consistent with the predictions of the jet-wind model (Table 6; case 2). [*See the electronic edition of the Journal for a color version of this figure.*]

4.2.3. *Alternative Explanations for Extra Light*

We note that there are three observational details that do not fit the generally used template SN 1998bw:

1. Rapid intensity decay: The *J*-band flux on 2002 February 9 is far below the prediction of SN 1998bw. While there exist SNe with rapidly decaying light curves, this faster decline applies only for times $t > 80$ days. These SNe are thought to possibly produce less Ni but more Ti. In the case of GRB 011121, the observed faster decay happened within less than 60 days after the maximum and thus cannot be explained with a low Ni production.

2. Atypical color evolution: SN decay slower at longer wavelength, e.g., SN 1998bw or SN 2002ap. The light curve of GRB 011121 shows that the brightness decay in the *J* band is very rapid. Moreover, the *HST* data demonstrate that the decay in the *R* band is not only slower than that in the *J* band, but also the *V*-band decay is slower than the *R*-band decay. Thus, in GRB 011121 the color dependence is just inverted relative to an SN: the longer the wavelength, the faster the decay.

3. Different SED: The excess light in GRB 011121 is substantially bluer than that of SN 1998bw, as already noted by Garnavich et al. (2003). This is most easily recognized in the different *k*-values for the different filters: while $k = 0.86 \pm 0.14$ for the R_C band (see previous section; excluding the *HST* data), we find $k = 1.10 \pm 0.50$ in the *V* band and $k = 0.40 \pm 0.03$ in the *J* band.

We investigated the alternative to the SN interpretation, namely, a dust echo due to scattered light (Esin & Blandford 2000; Waxman & Draine 2000; Reichart 2001). In the absence of extinction within the host galaxy, as in the case of GRB 011121, the dust echo is expected to be bluer than prescattered light, just as observed. This would suggest that a thermal dust echo is clearly ruled out since it would peak in the NIR band (Reichart 2001). However, in the dust echo scenario there seems to be a severe problem with the temporal evolution. Dust echoes due to scattered light do not peak as sharply as thermal dust echoes or SNe (Reichart 2001). The time dependence comes from the angular dependence of the escape probability of the scattered photons. Using the values of the differential escape probability as presented by Esin & Blandford (2000), we find that the inferred temporal decay should be much smaller than the observed decay rate after the bump maximum. Other alternatives are neutrons in the blast wave (Beloborodov 2003), the scenario of a

refreshed relativistic shock in the GRB outflow caused by the wind profile of the GRB progenitor (Ramirez-Ruiz et al. 2001), the shell collision model (Kumar & Piran 2000), or continuous injection (Björnsson et al. 2002). However, these scenarios are not yet detailed enough to be tested against observational data.

4.3. *The Break in the Light Curve*

One might be concerned that the break in the *R*-band light curve happens at an intensity level that just corresponds to the *R*-band brightness of the host. However, this is chance coincidence and only applies to the *R* band. There are three arguments in favor of the break being unaffected by the host brightness: (1) A subtraction of a constant flux could potentially produce a jump in the light curve, but no break with increasing deviation at later times. (2) The *R*-band brightness of the host is the brightness integrated over the area of the host. In contrast, the additional flux that the host would add to the point-spread function area of the afterglow is at least a factor of 4 smaller. Thus, if the break would have been " produced " by a wrong host subtraction, it would occur at a level nearly 2 mag fainter. (3) The brightness of the host is different in different filter bands ($V-J = 1.3$ mag). This color is different than that of the afterglow ($V-J = 2.45$ mag; both values not corrected for extinction). Yet, the break is found at the same *time* in *all* filter bands, irrespective of the relative brightness of the host to the afterglow.

The break time t_b we deduce has a 1 σ error of 0.5 days so that one might tentatively conclude that any break occurred between about 1 and 2 days after the burst. Whereas a break at very early times ($t < 1$ day) is excluded by the data obtained by Price et al. (2002) and Garnavich et al. (2003), a break at $t = 2$–3 days could be hidden by the bright SN component. The following discussion relies on the deduced break time of $t_b \approx 1.3$ days.

According to Livio & Waxman (2000), for a jetted explosion into wind-blown surroundings with an $n(r) \sim r^{-2}$ gas density profile it is

$$\Theta_{\rm jet} \approx 0.11 \left(\frac{E_{53}}{\dot{M}_{-5}/v_{w,3}}\right)^{-1/4} \left(\frac{t_b}{1+z}\right)^{1/4}, \qquad (3)$$

where $\dot{M}_{-5}$ is the mass-loss rate of the star in units of 10^{-5} $M_\odot$ yr^{-1}, $v_{w,3}$ is the wind velocity in units of 10^3 km s^{-1}, and E_{53} is the isotropic equivalent energy of the fireball in units of 10^{53} ergs. We introduced a factor $(1+z)$ in order to correct for the redshift. Using $z = 0.36$, $E_{53} = 0.27$ and assuming $\dot{M}_{-5}/v_{w,3} = 1$, we obtain $\Theta_{\rm jet} \sim 9^\circ$. This corresponds to a beaming factor ($b \approx 2/\Theta_{\rm jet}^2$) of about 100.

Usually it is assumed that E_{53} can be approximated by the isotropic equivalent energy release E_γ in the gamma-ray band during the burst phase. According to Garnavich et al. (2003), for GRB 011121 it was $E_\gamma = 0.27 \times 10^{53}$ ergs (see also § 2.1). After correcting for the beaming factor this gives an energy release of about 3×10^{50} ergs, in agreement with the typical energy releases of GRBs (Frail et al. 2001).

Given the many multifilter observations during the first 4 days (Table 1), we have constructed broadband spectra from the optical to the NIR region. These are shown in Figure 11 with a separation of about 24 hr between each other. The SEDs of the first 4 days are consistent with a $\beta = 0.70$ power law. This suggests that the break in the light curve was achromatic, in agreement with the predictions of the jet model. We note in passing that we do not see β to evolve toward an asymptotic value of 1.1 as has been argued by Dado et al. (2002b) and assumed for the cannonball interpretation of the GRB 011121 afterglow light curve.

4.4. *The Host Galaxy*

4.4.1. *Morphology*

Images in *R*, *V*, and *J* show that the host galaxy starts affecting the brightness estimate of the afterglow already after 2001 November 24. We have therefore taken the *J*-band image from February 9 to model the shape and intensity distribution of the host galaxy in order to subtract the host flux from the earlier images. The February 9 exposure consists of two subexposures, each with 30 minute exposure time and taken at a mean seeing of 0.″45 and 0.″55, respectively. We used the 0.″45 part and modeled the host galaxy using a bulge component

$$I_{\rm bulge}(R) = I_{\rm bulge,0} \exp\left[-7.67\left(\frac{R}{R_e}\right)^{1/4}\right] \qquad (4)$$

and a disk component

$$I_{\rm disk}(R) = I_{\rm disk,0} \exp\left(-1.68\,\frac{R}{R_e}\right). \qquad (5)$$

For each of these two components, the four parameters $I_{\rm bulge,0}$ ($I_{\rm disk,0}$), effective radius R_e, position angle (P.A.), and eccentricity ($e = [1-(b/a)^2]^{1/2}$) are derived using the IRAF/SPP package GIM2D (Simard 1998). The resulting fit parameters are as follows:

1. Bulge component: $I_{\rm bulge,0} = 14.78$ mag arcsec^{-2}, $R_e = 5.0$ pixels, $e = 0.19$, P.A. $= -41^\circ$.
2. Disk component: $I_{\rm disk,0} = 22.18$ mag arcsec^{-2}, $R_e = 19.5$ pixels, $e = 0.19$, P.A. $= -46^\circ$.

The eccentricity derived from the galaxy profile in the *J* band corresponds to an inclination of $\sim 10^\circ$.

The fit to the radial profile is given in Figure 16. To subtract the host galaxy emission from the images taken in 2001 November/December, this model of the host galaxy was convolved with the corresponding seeing of each image and then subtracted. For filters other than *J*, the total brightness of the model was modified to achieve good subtraction in the corresponding band; i.e., the normalization was varied to minimize the residuals. Aperture photometry on the subtracted images was then applied to obtain the magnitudes of the afterglow (see Table 1 and Fig. 9).

Using the model parameters given above and integrating over the galaxy, we obtain the following apparent magnitudes of the host galaxy: $J = 19.1 \pm 0.1$, $R = 20.1 \pm 0.1$, and $V = 20.4 \pm 0.1$.

The decomposition of the surface brightness profile of the galaxy into a disk and a bulge component shows that the bulge dominates within the inner 0.″5 only. The bulge contributes about 22% to the total light. This can be interpreted as an Sbc morphological type. The observed brightnesses of the host galaxy in the *V*, *R*, and *J* bands correspond, after correction for foreground absorption and applying the *k*-correction, to absolute magnitudes of -22.58 ± 0.53, -22.24 ± 0.24, and -22.09 ± 0.25, respectively. This is at the very bright end of the range populated by spirals (e.g.,

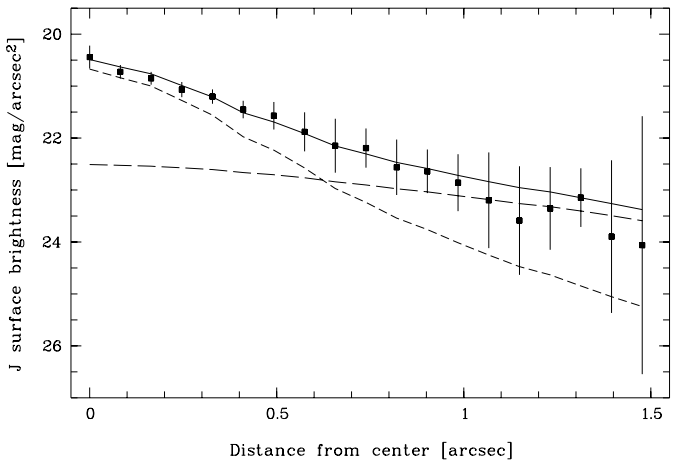

FIG. 16.—Surface brightness profile of the host galaxy of GRB 011121 in the J band, measured on the 2002 February 9 image (first part) at $0''.45$ seeing with a plate scale of $0''.147$ pixel^{-1} (two data points per pixel). The abscissa is the distance from the center measured as $(a^2 + b^2)^{1/2}$, with a and b being the major and minor axes of the galaxy, respectively. The dashed line denotes the bulge component, the long-dashed line the disk component, and the solid line the sum of both components.

Binggeli, Sandage, & Tammann 1988); the host galaxy of GRB 011121 is thus among the brightest 5% Sbc galaxies.

The GRB happened at an offset of $0''.9$ from the center of the host galaxy (as measured on a VLT image taken at $0''.6$ seeing), corresponding to a physical distance of 9 kpc (see also Ryder et al. 2001). The above-derived disk radius is $R_e = 29$ kpc. This offset location of the GRB with its SN is consistent with the general SN picture, as well as with offsets found for earlier GRBs (Bloom, Kulkarni, & Djorgovski 2002a).

4.4.2. *The Star Formation Rate*

Using the extinction-corrected line fluxes of [O II] and Hα (Table 5) and the relations given by Kennicutt (1998), i.e., $\mathrm{SFR}(\dot{M}\ \mathrm{yr}^{-1}) = 1.4 \times 10^{-41} L(\mathrm{O\ II})$ and $\mathrm{SFR}(\dot{M}\ \mathrm{yr}^{-1}) = 7.9 \times 10^{-42} L(\mathrm{H}\alpha)$, we deduce a star formation rate of 1.2 and 0.72/0.61 $M_\odot\ \mathrm{yr}^{-1}$, respectively. In contrast, Subrahmanyan et al. (2001) derive a star formation rate of 13–70 $M_\odot\ \mathrm{yr}^{-1}$ from their radio detection of the host galaxy at 0.05 mJy and assuming a spectral slope of -0.5 between 1.4 and 8.5 GHz. The rate derived here is at the low end of the range found previously in GRB host galaxies. However, also for these earlier cases different results are obtained for different methods/lines, in particular also a large difference between radio versus optically based data (Vreeswijk et al. 2001).

We have no explanation for the fact that the host galaxy appears to be among the brightest 5% Sbc galaxies, and yet the derived star formation rate is rather low. In addition, the lack of clear evidence for dust in the GRB host along the line of sight is somewhat surprising in the SN picture, although there is also no strong intrinsic extinction in most previous GRB hosts.

5. CONCLUDING REMARKS

While our α- and β-values are consistent within the errors with those reported by Garnavich et al. (2003) and Price et al. (2002), the change in our values due to the discovery of the break and the evolution during the 4 days after the GRB leads to a preference of the jet-wind model. The observed break and its interpretation are in contradiction with the interpretation of the radio data by Price et al. (2002), suggesting a break at times later than 8 days after the GRB. We cannot offer a solution to this problem, as the break is observationally evident from a dozen of data points spread over several filter bands.

Our observations reveal a light-curve break at early times and the appearance of extra light at late times. The former is believed to be evidence for a collimated outflow (a fireball jet), whereas the latter could be due to SN light. Finally, the α-β relations favor a wind model (Table 6). The afterglow of GRB 011121 thus provides another case in support of the current standard paradigm of long-duration GRBs: the collapsar model (Woosley 1993; Hartmann & Woosley 1995) in which the birth of a black hole inside a rapidly rotating massive star is announced via jet formation, breakout, and propagation into a stellar environment that was shaped by the strong winds of the precollapse star. In fact, GRB 011121 is the first case, where all three signatures (jet break, wind density profile, and SN bump) have been found, while in earlier cases only two of these three ingredients could be found (e.g., Jaunsen et al. 2001). However, even with GRB 011121 this line of reasoning remains circumstantial, and many more afterglows have to be observed and better sampled than is presently the case to seriously establish the GRB-collapsar picture.

We are highly indebted to the ESO staff, in particular N. Ageorges, S. Bagnulo, H. Böhnhardt, V. Doublier, O. R. Hainaut, S. Hubrig, A. O. Jaunsen, E. Jehin, R. Johnson, A. Kaufer, M. Kürster, E. Mason, E. Pompei, and Th. Szeifert for prompt execution of the observing requests and all the additional effort related to that. We thank the anonymous referee for the extensive comments on the original version of this paper. J. Gorosabel acknowledges the receipt of a Marie Curie Research Grant from the European Commission, and J. M. Castro Cerón the receipt of an FPI doctoral fellowship from Spain's Ministerio de Ciencia y Tecnología. This work was supported by the Danish Natural Science Research Council (SNF), by "IUAP P5/36" Interuniversity Attraction Poles Programme of the Belgian Federal Office for Scientific, Technical and Cultural Affairs, and the Belgian Fund for Scientific Research (FWO). This research has made use of the USNOFS Image and Catalogue Archive operated by the United States Naval Observatory, Flagstaff Station (http://www.nofs.navy.mil/data/fchpix).

REFERENCES

Andersen, M. I., et al. 2000, A&A, 364, L54
Beloborodov, A. M. 2003, ApJ, 585, L19
Benetti, S., Turatto, M., Cappellaro, E., Danziger, I. J., & Mazzali, P. A. 1999, MNRAS, 305, 811
Bertin, E., & Arnouts, S. 1996, A&AS, 117, 393
Beuermann, K., et al. 1999, A&A, 352, L26
Binggeli, B., Sandage, A. R., & Tammann, G. A. 1988, ARA&A, 26, 509
Björnsson, G., Hjorth, J., Jakobsson, P., Christensen, L., & Holland, S. 2001, ApJ, 552, L121
Björnsson, G., Hjorth, J., Pedersen, K., & Fynbo, J. U. 2002, ApJ, 579, L59
Bloom, J. S., Kulkarni, S. R., & Djorgovski, S. G. 2002a, AJ, 123, 1111
Bloom, J. S., et al. 1999, Nature, 401, 453
———. 2002b, ApJ, 572, L45

Brown, M., Schommer, R., Olsen, K., Jannuzi, B., Dey, A., Fruchter, A., & Rhoads, J. 2001, GCN Circ. 1158 (http://gcn.gsfc.nasa.gov/gcn/gcn3/1158.gcn3)
Cardelli, J. A., Clayton, G. C., & Mathis, J. S. 1989, ApJ, 345, 245
Castro-Tirado, A. J., & Gorosabel, J. 1999, A&AS, 138, 449
Castro-Tirado, A. J., et al. 2001, A&A, 370, 398
Chevalier, R. A., & Li, Z.-Y. 2000, ApJ, 536, 195
Dado, S., Dar, A., & De Rujula, A. 2002a, A&A, 388, 1079
———. 2002b, ApJ, 572, L143
de Jong, R. S. 1996, A&A, 313, 45
Devillard, N. 2002, Eclipse User's Guide
Dickey, J. M., & Lockman, F. J. 1990, ARA&A, 28, 215
Drory, N. 2003, A&A, 397, 371
Esin, A. A., & Blandford, R. 2000, ApJ, 534, L151
Frail, D. A., et al. 2001, ApJ, 562, L55
Fryer, C. L., Woosley, S. E., & Hartmann, D. H. 1999, ApJ, 526, 152
Galama, T. J., et al. 1998, Nature, 395, 670
———. 2000, ApJ, 536, 185
Garnavich, P. M., et al. 2001, GCN Circ. 1273 (http://gcn.gsfc.nasa.gov/gcn/gcn3/1273.gcn3)
———. 2003, ApJ, 582, 924
Greiner, J., et al. 2001, GCN Circ. 1166 (http://gcn.gsfc.nasa.gov/gcn/gcn3/1166.gcn3)
Hartmann, D. H., & Woosley, S. E. 1995, Adv. Space Res., 15(5), 143
Heger, A., Fryer, C. L., Woosley, S. E., Langer, N., & Hartmann, D. H. 2003, ApJ, 591, 288
Hjorth, J., et al. 2003, Nature, 423, 847
Holland, S. T., et al. 2001, A&A, 371, 52
———. 2003, AJ, 125, 2291
Hurley, K., Cline, T., Guidorzi, C., Montanari, E., Frontera, F., & Feroci, M. 2001, GCN Circ. 1148 (http://gcn.gsfc.nasa.gov/gcn/gcn3/1148.gcn3)
Hurley, K., et al. 2002, GCN Circ. 1372 (http://gcn.gsfc.nasa.gov/gcn/gcn3/1372.gcn3)
Infante, L., Garnavich, P. M., Stanek, K. Z., & Wyrzykowski, L. 2001, GCN Circ. 1152 (http://gcn.gsfc.nasa.gov/gcn/gcn3/1152.gcn3)
Jaunsen, A. O., et al. 2001, ApJ, 546, 127
Kennicutt, R. C., Jr. 1998, ARA&A, 36, 189
Klose, S., et al. 2000, ApJ, 545, 271
Kumar, P., & Panaitescu, A. 2000, ApJ, 541, L9
Kumar, P., & Piran, T. 2000, ApJ, 532, 286
Landecker, T. L., et al. 1999, ApJ, 527, 866
Lazzati, D., Rossi, E., Covino, S., Ghisellini, G., & Malesani, D. 2002, A&A, 396, L5
Lazzati, D., et al. 2001, A&A, 378, 996
Leibundgut, B. 1990, A&A, 229, L1
Livio, M., & Waxman, E. 2000, ApJ, 538, 187
Masetti, N., et al. 2003, A&A, 404, 465
Mészáros, P. 2002, ARA&A, 40, 137
Mészáros, P., Rees, M. J., & Wijers, R. A. M. J. 1998, ApJ, 499, 301
Patat, F., et al. 2001, ApJ, 555, 900
Phillips, M. M., Krisciunas, K., Garnavich, P. M., Holland, S., Jha, S., Stanek, K. Z., & McCarthy, P. 2001, GCN Circ. 1164 (http://gcn.gsfc.nasa.gov/gcn/gcn3/1164.gcn3)
Piro, L. 2001a, GCN Circ. 1147 (http://gcn.gsfc.nasa.gov/gcn/gcn3/1147.gcn3)
———. 2001b, GCN Circ. 1149 (http://gcn.gsfc.nasa.gov/gcn/gcn3/1149.gcn3)
Piro, L., et al. 2001, GCN Circ. 1172 (http://gcn.gsfc.nasa.gov/gcn/gcn3/1172.gcn3)
Predehl, P., & Schmitt, J. H. M. M. 1995, A&A, 293, 889
Price, P. A., McCarthy, P., Fox, D. W., Koviak, K., & Bloom, J. S. 2001, GCN Circ. 1153 (http://gcn.gsfc.nasa.gov/gcn/gcn3/1153.gcn3)
Price, P. A., et al. 2002, ApJ, 572, L51
Ramirez-Ruiz, E., et al. 2001, MNRAS, 327, 829
Reichart, D. E. 2001, ApJ, 554, 643
Rhoads, J. 1999, ApJ, 525, 737
Rhoads, J. E., & Fruchter, A. S. 2001, ApJ, 546, 117
Rieke, G. H., & Lebofsky, M. J. 1985, ApJ, 288, 618
Ryder, S., Gunn, K., Seymour, N., Price, P. A., Schmidt, B. P., & Axelrod, T. S. 2001, GCN Circ. 1163 (http://gcn.gsfc.nasa.gov/gcn/gcn3/1153.gcn3)
Sari, R., Piran, T., & Halpern, R. 1999, ApJ, 519, L17
Sari, R., Piran, T., & Narayan, R. 1998, ApJ, 497, L17
Schlegel, D., Finkbeiner, D., & Davis, M. 1998, ApJ, 500, 525
Simard, L. 1998, in ASP Conf. Ser. 145, Astronomical Data Analysis Software and Systems VII, ed. R. Albrecht, R. N. Hook, & H. A. Bushouse (San Francisco: ASP), 108
Sokolov, V. V. 2002, in Gamma-Ray Bursts in the Afterglow Era, ed. E. Costa, F. Frontera, & J. Hjorth (Garching: ESO), 136
Stanek, K. Z., & Wyrzykowski, L. 2001, GCN Circ. 1160 (http://gcn.gsfc.nasa.gov/gcn/gcn3/1160.gcn3)
Subrahmanyan, R., Kulkarni, S. R., Berger, E., & Frail, D. A. 2001, GCN Circ. 1156 (http://gcn.gsfc.nasa.gov/gcn/gcn3/1156.gcn3)
Tinney, C., Stathakis, R., Cannon, R., & Galama, T. 1998, IAU Circ. 6896
van Paradijs, J., Kouveliotou, C., & Wijers, R. 2000, ARA&A, 38, 379
van Paradijs, J., et al. 1997, Nature, 386, 686
Vietri, M., & Stella, M. 1998, ApJ, 507, L45
———. 1999, ApJ, 527, L43
Vreeswijk, P. M., Fender, R. P., Garrett, M. A., Tingay, S. J., Fruchter, A. S., & Kaper, L. 2001, A&A, 380, L21
Waxman, E., & Draine, B. T. 2000, ApJ, 537, 796
Wei, D. M., & Jin, Z. P. 2003, A&A, 400, 415
Weiler, K. W., Panagia, N., Montes, M., & Sramek, R. A. 2002, ARA&A, 40, 387
Woosley, S. E. 1993, ApJ, 405, 273
Wyrzykowski, L., Stanek, K. Z., & Garnavich, P. M. 2001, GCN Circ. 1150 (http://gcn.gsfc.nasa.gov/gcn/gcn3/1150.gcn3)
Zeh, A., & Klose, S. 2003, ApJ, submitted
Zeh, A., Klose, S., Henden, A., & Greiner, J. 2003, GCN Circ. 2115 (http://gcn.gsfc.nasa.gov/gcn/gcn3/2115.gcn3)